Agricultural and Forest Meteorology 249 (2018) 176–186

Contents lists available at ScienceDirect

Agricultural and Forest Meteorology

journal homepage: www.elsevier.com/locate/agrformet

Modeling vegetation green-up dates across the Tibetan Plateau by including both seasonal and daily temperature and precipitation

Ruyin Cao[a,*], Miaogen Shen[b,c,**], Ji Zhou[a], Jin Chen[d]

[a] School of Resources and Environment, University of Electronic Science and Technology of China, 2006 Xiyuan Avenue, West Hi-tech Zone, Chengdu, Sichuan 611731, China
[b] Key Laboratory of Alpine Ecology and Biodiversity, Institute of Tibetan Plateau Research, Chinese Academy of Sciences,16 Lincui Road , Beijing 100101, China
[c] CAS Center for Excellence in Tibetan Plateau Earth Sciences,16 Lincui Road, Beijing 100101, China
[d] State Key Laboratory of Earth Surface Processes and Resource Ecology, Beijing Normal University, Beijing, 100875, China

ARTICLE INFO

Keywords:
Alpine vegetation
Asymmetric warming
Daytime mean temperature
Phenological model
Remotely sensed phenology
Start of growing season

ABSTRACT

Shifts in vegetation phenology induced by climate change are substantially modifying various ecosystem processes, and those changes can in turn affect weather and climate systems. Realistic modeling of spring vegetation green-up is critical to improving process-based ecosystem models of the Tibetan Plateau (TP) and for better understanding of the coupling between TP terrestrial biophysical processes and the Asian monsoon system. However, no model is available for simulating the vegetation green-up date (VGD) across the entire TP. In this study, we first assessed the ability of several existing state-of-the-art phenological models to estimate VGD across the TP. We then modified the existing models by adding environmental constraints identified by partial least-squares analyses. The modified models simulated VGDs with lower estimation errors than other models (Mean absolute error: 8.2 days vs. 8.7–12.9 days; $P < 0.01$, *t*-test). Moreover, although our model captured the inter-annual variations in VGD better than any previous model, the correlation coefficient between predicted and remotely sensed VGDs was still low, especially in the western TP. This study revealed the necessity of considering multiple factors in VGD models and highlighted the challenge of developing models that will better represent phenology in future ecosystem models.

1. Introduction

Vegetation green-up date (VGD) characterizes the onset of photosynthetic activity on land and has important implications for terrestrial ecosystem processes, such as carbon and water cycling and the energy balance between the biosphere and atmosphere (Cleland et al., 2007; Forkel et al., 2015; Jeong et al., 2012; Keenan et al., 2014; Menzel and Fabian, 1999; Richardson et al., 2013; Wu et al., 2016). It is also considered to be the simplest and one of the most sensitive indicators of the response of vegetation to recent climate warming, especially at high latitudes and in high-altitude regions (Körner and Basler, 2010; Parmesan, 2006; Peñuelas et al., 2009; Vitasse et al., 2011; Walther et al., 2002; Zheng et al., 2016). The Tibetan Plateau (hereafter TP), covering an area of approximately 2.5×10^6 km^2 and with an average elevation higher than 4000 m, is the largest and highest alpine ecoregion in the world and has experienced extraordinary warming in the past four decades, during which the mean annual temperature has increased at a rate of 0.39 °C per decade (Deng et al., 2017). A growing number of studies have used ground records and satellite observations to study the temporal shifts of the VGD and the linkages of those shifts to climate on the TP (reviewed by Shen et al., 2015b). Shifts in spring vegetation phenology could induce changes in surface biophysical processes and further potentially affect the regional and eastern Asian climate (Zhang et al., 2011).

It is widely recognized that heat accumulation in the preceding period of time (preseason) is the main trigger of VGD on the cold TP (e.g., Piao et al., 2011; Shen et al., 2011). Investigators have also explored the influences on VGD of some other environmental factors, such as the winter temperature and its relationship to chilling effects (Yu et al., 2010), preseason precipitation (Shen et al., 2015a), photoperiod, and sunshine duration (Wang et al., 2015). For example, Yu et al. (2010) found that winter warming slowed the fulfillment of the chilling

* Corresponding author at: University of Electronic Science and Technology of China, School of Resources and Environment, 2006 Xiyuan Avenue, West Hi-tech Zone, 611731, Chengdu, China.
** Corresponding author at: Key Laboratory of Alpine Ecology and Biodiversity, Institute of Tibetan Plateau Research, Chinese Academy of Sciences,16 Lincui Road , Beijing 100101, China.
E-mail addresses: cao.ruyin@uestc.edu.cn (R. Cao), shen.miaogen@gmail.com (M. Shen).

https://doi.org/10.1016/j.agrformet.2017.11.032
Received 25 July 2017; Received in revised form 5 October 2017; Accepted 29 November 2017
Available online 12 December 2017
0168-1923/

requirement and consequently delayed spring phenology across the TP from the mid-1990s to 2006. That report, however, has stimulated a broad debate about whether there is a strong winter chilling effect on the TP. Some later studies have argued that warmer winters do not postpone spring phenology on the TP (e.g., Chen et al., 2015; Cong et al., 2017; Zhang et al., 2013). Besides the winter temperature, several studies have emphasized the important impacts of preseason precipitation on spring phenology in the dry areas of the TP and have suggested including this factor in climate-driven phenology models to improve phenology simulations (Shen et al., 2011; Shen et al., 2015a).

In addition to these seasonal climate variables, some recent studies have emphasized that VGD is affected by the asymmetric impacts of daytime and nighttime temperatures (Fu et al., 2016; Hanes, 2014; Piao et al., 2015; Rossi and Isabel, 2017; Shen et al., 2016). Piao et al. (2015) have suggested that spring phenology is more strongly related with daily maximum temperature than with daily minimum temperature over northern middle and high latitudes. Fu et al. (2016), on the basis of a manipulative experiment, have further indicated that the impact of daytime temperatures on the leaf unfolding phenology of three temperate tree species is three times that of nighttime temperatures. In contrast, Shen et al. (2016) correlated VGD with daily maximum and minimum temperatures, and they found a stronger impact of minimum temperatures on the TP and hypothesized this as a low-temperature constraint. These discoveries have been crucial for understanding what temperature really drives spring phenology on the TP.

Despite this progress, however, it is still unclear how VGD across the TP is codetermined by temperature at both seasonal (winter vs. spring) and diurnal (daytime vs. nighttime) time scales and by preseason precipitation. More importantly, little is known about whether, and to what extent, including these reported environmental cues might improve phenological models and yield more realistic phenological predictions for the TP. We found that there have been few previous efforts to model VGD on the TP, and those limited efforts have been made for only a few species at several separate sites (Chen et al., 2015) that could not represent the entire TP. More accurate prediction of VGD requires the inclusion of essential mechanisms in the phenological model without overfitting model coefficients (Linkosalo et al., 2008). Previous studies have revealed correlations between environmental cues and VGDs, but there remains a gap to incorporate such correlations for an improvement of VGD predictions on the TP.

To fill knowledge gaps, we first investigated the combined effect of multiple climate variables on satellite-derived VGD (2001–2015) across the TP. We then assessed the performance of several existing state-of-the-art, climate-driven phenological models in predicting VGD. We then developed a new phenological model involving multiple environmental cues to improve VGD simulations across the entire TP.

2. Materials and methods

2.1. Retrieving VGDs using satellite observations

VGDs across the TP during 2001–2015 were estimated on the basis of a time series of normalized difference vegetation index (NDVI) values. Raw NDVI values were calculated from the nadir bidirectional reflectance distribution function (BRDF)-adjusted reflectance observed by the Moderate Resolution Imaging Spectroradiometer (MODIS) (Product No. MCD43A4; Schaaf et al., 2002). The MCD43A4 dataset has a composited 8-day and 500-m temporal-spatial resolution and was available from the website of the National Aeronautics and Space Administration (http://reverb.echo.nasa.gov/reverb). We then performed some necessary preprocessing of the generated raw time-series NDVI data to reduce noise in the time series: (1) the BRDF-albedo quality flag (Product No. MCD43A2) was used to identify winter NDVI values contaminated by the presence of snow or ice; (2) these contaminated NDVI data were replaced by median values of the uncontaminated NDVI values between the previous November and the following March of all years (Zhang et al., 2006); (3) remaining gaps in the time series were linearly interpolated, and the time series was further smoothed by a three-point median-value filter, as suggested by the official User Guide (http://www.bu.edu/lcsc/files/2012/08/MCD12Q2_UserGuide.pdf).

After preprocessing, the NDVI time-series was fitted to a logistic function. VGD was then defined as the date when the rate of change of the curvature of the fitted function reached its first local maximum (for details, see Zhang et al., 2003). This method actually captures the time of the initial rapid increase of vegetation greenness and has been widely validated and used (e.g., Ganguly et al., 2010; Zhang et al., 2006; Zhu et al., 2012). Only the pixels with obvious seasonal changes were included for analysis. These pixels were identified according to the following criteria: the annual NDVI maximum occurred between June and September; the average NDVI during July–September was larger than 0.1; and the July–September average exceeded 1.2 times the average NDVI during January–March (Cao et al., 2015; Shen et al., 2014).

2.2. Climate data

The China Meteorological Forcing Dataset was used to analyze the relationships between VGD and climate factors for each pixel. This dataset was provided by the Data Assimilation and Modeling Center for Multi-spheres, Institute of Tibetan Plateau Research, Chinese Academy of Sciences (Chen et al., 2011; Yang et al., 2010). Air temperature and precipitation data in that dataset have a spatial resolution of $0.1^\circ \times 0.1^\circ$ and a temporal resolution as short as 3 h. Air temperatures were produced by merging station meteorological observations made by the China Meteorological Administration (CMA) and the corresponding Princeton forcing data (Sheffield et al., 2006). Precipitation data were produced from CMA station observations, Tropical Rainfall Measuring Mission satellite precipitation analysis data (3B42; Huffman et al., 2007), and APHRODITE (Asian Precipitation − Highly Resolved Observational Data Integration Towards Evaluation of Water Resources) precipitation data (Yatagai et al., 2009).

2.3. Statistical analyses

We performed partial least-squares regressions (PLSRs) to evaluate the influences of multiple climate factors on inter-annual variations of the VGD. Compared with ordinary least-squares multiple regression, PLSR is more useful when the sample size is small and there is multicollinearity among the independent variables (Wold, 1995). The climatic factors in our PLSR analyses included daytime mean temperature ($T_{daytime}$) and daily minimum temperature (T_{min}) during the preseason period, preseason accumulated precipitation (AP), and winter daily mean temperature (T_{winter}). $T_{daytime}$ was calculated as the mean of the four temperatures recorded during successive 3-h time intervals from 8:00 AM to 8:00 PM The duration of the preseason used to calculate $T_{daytime}$ was determined to be the period of time preceding the multiyear average VGD during which the VGD was most correlated with $T_{daytime}$. We constrained this length of time to be 15–90 days in increments of 15 days to suppress the potential influence of occasionally abnormal temperatures. The preseason length for T_{min} was determined in a similar way. The time interval for calculating AP extended from 1 January to the multiyear average VGD. T_{winter} was calculated as the daily mean temperature from October 1 of the previous year to January 31 of the given year.

We quantified the influence of each climate factor on the VGD on the basis of two evaluation indicators from the PLSR analyses. One was the model coefficient (MC) in the regression model. A positive or negative MC for a climate factor indicated that the climate factor was positively or negatively correlated, respectively, with VGD. The other was the variable importance on PLSR projection (VIP), which is a metric of the ability of each climate factor to explain the variance of the VGD (Yu et al., 2010). A climate factor with a VIP score greater than 1

Table 1
Descriptions of the phenological models used in this study.

Model	Model equations Parameters (constrained range)
SW1	$S_f = \sum_{t_s}^{t_b} \max(0, T_{daily} - T_h) \geq F^*$
	Parameters: t_s (1, VGD_{min}), T_h (0,5), F^*(0,1500)
SW2	$S_f = \sum_{t_s}^{t_b} \max(0, T_{daytime} - T_h) \geq F^*$
	Parameters: t_s (1, VGD_{min}), T_h (0,5), F^*(0,1500)
SW3	$S_f = \sum_{t_s}^{t_b} [ka*\max(0, T_{daytime} - T_h) + kb \times \max(0, T_{nighttime} - T_h)] \geq F^*$
	Parameters: t_s (1, VGD_{min}), T_h (0,5), F^*(0,1500), Ka (0.5,1.0), Kb (0,0.5)
SEQ	$S_c = \sum_{t_w}^{t_1} \begin{cases} 1 & T_{daily} < T_c \\ 0 & T_{daily} \geq T_c \end{cases} = C^*\#XPS\#amp;\ S_f = \sum_{t_1}^{t_b} \begin{cases} T_{daily} - T_h & T_{daily} > T_h \\ 0 & T_{daily} \leq T_h \end{cases} \geq F^*$
	Parameters: T_c (−10,5), C^*(0.240), T_h (0,5), F^*(0,1500)
PAR	$S_c = \sum_{t_w}^{t_b} \begin{cases} 1 & T_{daily} < T_c \\ 0 & T_{daily} \geq T_c \end{cases} \#XPS\#amp;\ S_f = \sum_{t_s}^{t_b} \min\left(1, \frac{S_c}{C^*}\right) \times \max(0, T_{daily} - T_h) \geq F^*$
	Parameters: T_c (−10,5), C^*(0.240), T_h (0,5), F^*(0,1500)
TPP	$S_f = \sum_{t_s}^{t_b} \max(0, T_{daytime} - T_h) \geq F^*\#XPS\#amp;\ S_P = \sum_{1}^{t_b} P_t \geq P^*$
	Parameters: t_s (1, VGD_{min}), T_h (0,5), F^*(0,1500), P^*(0.300)
Modified_SW	
SW2	$S_f = \sum_{t_s}^{t_b} \max(0, T_{daytime} - T_h) \geq F^*$
	t_s (1, VGD_{min}), T_h (0,5), F^*(0,1500)
*SW2_*$T_{daytime}$	$S_f = \sum_{t_s}^{t_b} \max(0, T_{daytime} - T_h) \geq F^* + ka \times \sum_{t_s}^{t_b} \max(5, T_{daytime} - T_h)$
	t_s (1, VGD_{min}), T_h (0,5), F^*(0,2500), ka(0,2)
*SW2_*T_{min}	$S_f = \sum_{t_s}^{t_b} \max(0, T_{daytime} + ka \times (\frac{1}{t_b - t_s + 1} \times T_{min}) + kb - T_h) \geq F^*$
	t_s (1, VGD_{min}), T_h (0,5), F^*(0,2500), ka(−1,1), kb(0.15)
*SW2_*T_w	$S_f = \sum_{t_s}^{t_b} \max(0, T_{daytime} - T_h) \geq F^* + ka \times \frac{1}{(31 - t_w)} \sum_{t_w}^{31} T_{daily}$
	t_s (1, VGD_{min}), T_h (0,5), F^*(0,2500), ka(-100,100)
SW2_AP	$S_f = \sum_{t_s}^{t_b} \max(0, T_{daytime} - T_h) \geq F^* + ka \times \sum_{1}^{t_b} P_t$
	t_s (1, VGD_{min}), T_h (0,5), F^*(0,2500), ka(−500,500)
Statistical	$VGD = PLSR(T_{daytime}, T_{min}, T_w, AP)$,five parameters[a]

Notes: S_f is heat accumulations; S_c is chilling accumulations; T_{daily} is daily mean temperature; $T_{daytime}$ and $T_{nighttime}$ represent daytime and nighttime mean temperature, respectively; T_h and T_c are the base temperature required by the processes of heat accumulations and chilling accumulations; F^* represents the critical sum of required heat requirement units and C^* is the critical sum of required chilling requirement units; VGD_{min} is the multiyear minimum VGD for each pixel; t_s is the starting date for heat accumulations; t_b is the date when VGD occurs; t_w is defined as −90 to indicate October 1 of the previous year; ka and kb are the scale parameters to be calibrated. P_t is daily accumulated precipitation; P^* represents the critical sum of precipitation accumulations units. Max() returns the larger of the value in parenthesis.

[a] PLSR has five parameters, including an intercept term.

can be considered to be relatively important among the variables in the regression model according to the general "greater than one" criterion (Wold, 1995). Because the statistical analyses were conducted at the pixel level, the spatial resolution of the satellite-derived VGD was scaled up to 0.1° × 0.1° to match the resolution of the climate data. All variables were standardized to make each variable have a mean value of 0 and a standard deviation of 1 before PLSRs. The standardization and PLSRs analyses were implemented by using the zscore and plsregress functions in the Matlab version 2014 software (The MathWorks, Inc., Natick, MA, USA).

2.4. Phenological models

We first assessed the abilities of several existing state-of-the-art phenological models (models 1–3 below) to estimate VGDs throughout the TP. We then modified the existing models by adding constraints identified in the PLSR analysis.

2.5. Spring warming (SW) models

An SW model considers only the influence of spring temperature and assumes that VGD occurs when accumulated preseason temperature, designated the heat accumulation, reaches a critical sum of forcing units. We considered heat accumulation measured as three kinds of temperature: daily mean temperature (SW1) which is widely used in the traditional spring warming models (e.g. Botta et al., 2000), daytime mean temperature (SW2) as suggested by Piao et al. (2015), and daytime and nighttime mean temperature with different weights for day and night (SW3) (Fu et al., 2016). Table 1 provides details of the model equations.

2.6. Chilling-forcing models

This type of model assumes that in addition to an accumulation of heat, plants also need a sequence of low-temperature days (i.e., a chill

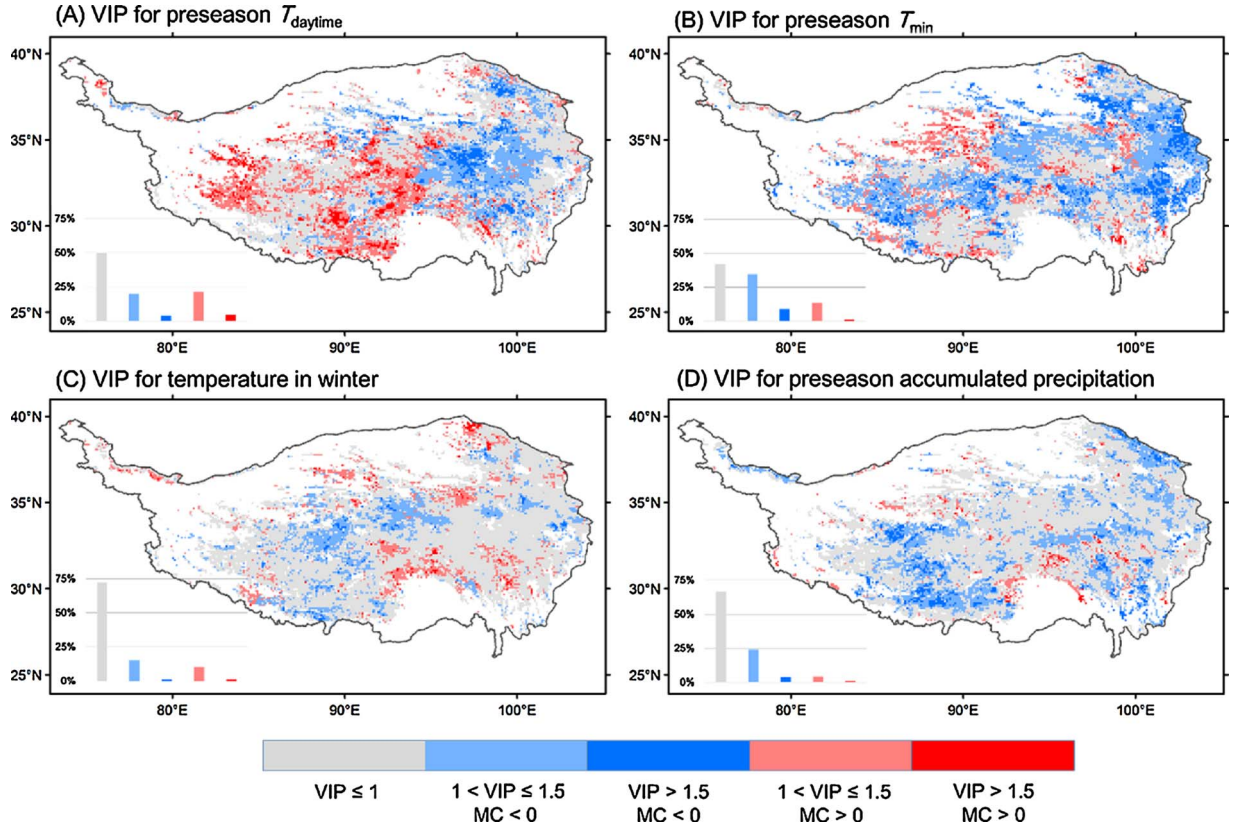

Fig. 1. Variable importance based on the PLSR projection (VIP) for (A) preseason daytime mean temperature ($T_{daytime}$), (B) preseason daily minimum temperature (T_{min}), (C) winter mean temperature (from October 1 of the previous year to January 31 of the given year), and (D) preseason accumulated precipitation (*AP*). Preseason lengths for different climate variables are explained in the Materials and methods section. VIP is a metric of the importance of each climate variable for vegetation green-up date (VGD). A climate variable with a VIP > 1 can be considered to be important among all variables for VGD. A positive or negative model coefficient (MC) indicates a positive or a negative correlation, respectively, with VGD.

requirement) to move from endodormancy to ecodormancy (Fu et al., 2015; Körner and Basler, 2010; Murray et al., 1989). We tested two chilling-forcing models. The first was a sequential model (SEQ in Table 1), which assumed that heat accumulation relevant to vegetation green-up started only after a sufficient number of low-temperature days (Chuine et al., 1998; Kramer, 1994). The second was a parallel model (PAR in Table 1), which assumed that both heating and chilling requirements accumulated concurrently, and that there was a negative correlation between the required amount of heat and the accumulated chilling (Chuine et al., 1998).

2.7. Temperature-precipitation parallel (TPP) model

The TPP model considered a water requirement for VGD in addition to a heat requirement. It assumed that the accumulated preseason precipitation had to reach a critical sum of precipitation units (Chen et al., 2014). As suggested by previous studies, precipitation is crucial for the vegetation green-up of arid and semi-arid grasslands (Chen et al., 2015; Shen et al., 2011). In the TPP model, we employed daytime mean temperature for heat accumulation.

2.8. Modified_SW models

We developed a new phenological model by modifying the spring warming model (called Modified_SW). Modified_SW consists of a group of five submodels. The five submodels were designated *SW2*, *SW2_*$T_{daytime}$, *SW2_*T_{min}, *SW2_*T_w, and *SW2_AP* (see equations in Table 1), respectively. Which submodel was applied to a pixel depended on the constraint identified by the PLSR analyses for that pixel. Totally, all vegetation pixels were classified into five cases, and each submodel was employed to deal with one case.

Cases 1 and 2: When the $T_{daytime}$ yielded the maximum VIP score for a pixel, the pixel was assigned to Case 1 or Case 2 if the MC in the PLSR was negative or positive, respectively. A positive MC suggests that VGD is delayed by an increase of $T_{daytime}$, a pattern that a spring warming model cannot capture. We thus considered higher $T_{daytime}$ as a stress on VGD in the *SW2_* $T_{daytime}$ *model*. The *SW2* and *SW2_* $T_{daytime}$ submodels were applied in Case 1 and Case 2, respectively.

Case 3: A pixel was assigned to Case 3 if T_{min} yielded the maximum VIP score. The *SW2_T* $_{min}$ submodel was applied in this case. We assumed that the lower the nighttime temperature, the more the efficiency of accumulated daily heating was reduced.

Cases 4 and 5: A pixel was assigned to Case 4 if the winter mean temperature (T_w) yielded the maximum VIP score and to Case 5 if the preseason accumulated precipitation (*AP*) yielded the maximum VIP score. The *SW2_*T_w and *SW2_AP* submodels were applied to a pixel in Case 4 and Case 5, respectively. In these submodels, we assumed that the total heat requirement was affected by T_w or *AP*.

Using these five submodels, we were able to deal with all vegetation pixels across the TP. Here, two points should be noted regarding the submodels. First, which submodel is applied to a pixel is according to the variable importance (i.e. VIP score) from PLSRs, but using PLSRs to determine correlations is based on the assumption that all variables are linearly correlated with VGD which should be kept in mind. In the Modified_SW model, we did not use the regression equations from PLSRs to directly construct the submodels but employed PLSRs only for climate variable selections. Numbers of previous studies have suggested the correlations between VGD and climate variables (e.g., temperature and precipitation) on TP from the PLSRs method (Yu et al., 2010) or the partial correlation analysis (Shen et al., 2016). In addition, our results showed that each submodel actually significantly improved VGD simulations compared with other existing models (see Figs. 4 and 6 in the

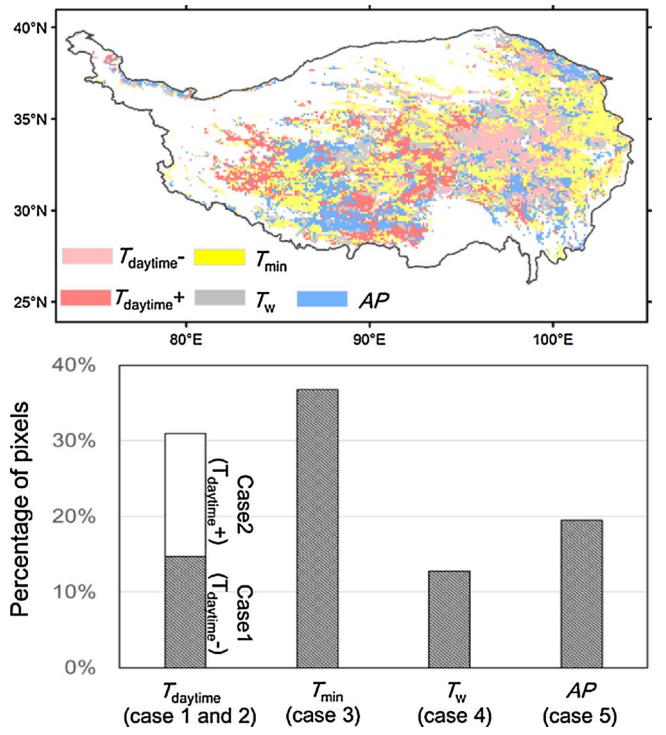

Fig. 2. Spatial distribution of the most important climate variables identified by the maximum VIP score in PLSR (upper panel), and percentages of pixels for each climate variable that shows the maximum VIP (lower panel). Here, the variable $T_{daytime}$ is further divided into two cases, $T_{daytime}-$ and $T_{daytime}+$, which indicate a negative or a positive correlation, respectively, with $T_{daytime}$. We used the each of the five submodels of the Modified_SW to deal with VGD simulations for each case of the five cases, respectively (see Materials and methods section).

results section), suggesting that using PLSRs for variable selections is an acceptable method. Understanding the exact relationship between various climate variables and VGD is the ultimate objective but remains a great challenge. Second, we added, at most, one climate factor in each submodel besides the variable $T_{daytime}$ in the original spring warming model (Table 1). We also tried to involve more climate factors (e.g., $T_{daytime}$, T_{min}, and *AP*) in one model to simulate VGD, but we found that a model with more parameters did not perform better (Fig. S1), probably because of overfitting of model coefficients (Linkosalo et al., 2008). We also tested the performance of a VGD multiple regression statistical model generated by PLSR.

Photoperiod were excluded in this analysis, because photoperiod has been found to play a weak role in regulating VGD on the TP (Wang et al., 2015). Besides, the period for heat accumulation was not fixed but was allowed to change in the models. This may implicitly account for photoperiod requirement to some extent (Migliavacca et al., 2012, Yang et al., 2012), since the starting date for heat accumulation occurs mainly during day of year 75–120 (Fig. S2) during which the day length is above 12 h on the plateau (the day length was calculated from an online program: http://solardat.uoregon.edu/SolarPositionCalculator.html).

2.9. Model calibration and validation

Because all the process-based phenological models had at least three parameters to be calibrated, we employed a simple genetic algorithm to search for the global optimum in a constrained parameter space (Table 1). The cost function was defined as the root mean square error between the satellite-derived VGD and the VGD simulated by the phenological model. Source codes of the genetic algorithm were taken from the website (www.ncnr.nist.gov/staff/dimeo/idl_programs.html).

We adopted the method of leave-one-out cross validation to evaluate each phenological model. Every time we chose data from one year from the total of 15 years, and we used data from that year to validate the phenological model that was calibrated with data from the other 14 years. Model errors were quantified by the mean absolute error (MAE) between simulations and satellite-derived VGDs. Pearson correlation coefficients were used to determine whether the simulations could capture the temporal variations of VGD. We did not use the Akaike Information Criterion (AIC), which has been used as an indicator in previous studies (e.g., Yang et al., 2012; Chen et al., 2015), because we found that the AIC gave inappropriate model evaluations in some cases (see Discussion).

3. Results

PLSR analyses indicated that preseason T_{min} yielded a VIP score > 1 for the greatest number of pixels (approximately 60% of pixels), the implication being that T_{min} among the four climate variables had the strongest impact on VGD (Fig. 1B). Furthermore, for 40% of the pixels the VGD was negatively correlated with T_{min} (i.e., MC < 0); this was about twice the percentage of pixels with a positive correlation between VGD and T_{min}. In contrast, the numbers of pixels with a positive or negative correlation between VGD and preseason $T_{daytime}$ were similar (Fig. 1A). Positive correlations for $T_{daytime}$ were observed mainly in the northwest and southwest of the TP, whereas negative correlations occurred mainly in the central and eastern TP. T_w had less effect than preseason temperature on VGD: approximately 25% of pixels had a VIP score > 1 (Fig. 1C). Moreover, we found that, between VGD and T_w, more pixels had a negative correlation. This result suggested that VGD probably occurred earlier with an increase of T_w, a pattern that is inconsistent with the findings of Yu et al. (2010), who reported that winter warming delayed spring phenology across the TP. We found a distinctly negative correlation between VGD and *AP*, mostly in the southwestern and northern TP; only a few pixels showed a positive correlation (Fig. 1D). This result suggests that increasing water availability by precipitation could advance the VGD.

We compared the VIP scores of the four climate variables and identified the key driving factor for each pixel based on the criterion of maximum VIP score. The results (Fig. 2) showed that four variables, $T_{daytime}$, T_{min}, T_w, and *AP*, were the main driving factors for approximately 31%, 36%, 13%, and 20% of the pixels, respectively. These results suggested that VGD was codetermined by multiple climate variables across the TP, and VGD simulations in this large alpine ecoregion could probably be improved by involving the key driving mechanism in the phenological model at the proper place. We further distinguished the positive and negative correlations of $T_{daytime}$ with VGD, which accounted for 16.3% and 14.7% of pixels, respectively. We therefore used the five submodels in the Modified_SW model to deal with VGD simulations for each case (Table 1 and Fig. 2). In addition, we examined whether there is an association between submodels and different vegetation types. On average, VGD for forests (Broadleaf and Needleleaf) tended to involve the variable of T_{min} and approximately 50% forest pixels employed the T_{min}-based submodel (i.e. case 3 in Fig. S3B), whereas grasslands, particularly steppes, were more likely to be constrained by higher $T_{daytime}$ compared with forests for VGD simulations (case 2 in Fig. S3B).

Fig. 3 showed the MAE between satellite-derived VGDs and VGDs simulated by various phenological models. We found that the Modified_SW model had the lowest average MAE (8.2 days) of the VGD simulations, and the MAEs of > 20% of the pixels were < 6 days (Fig. 3G). Among the three forms of SW models, the mean MAE of the SW1 model based on daily mean temperature was the largest (10.5 days), the suggestion being that the heating requirement for VGD was fulfilled primarily by daytime temperature across the TP (Fig. 3A). The SW3 model performed slightly better than the SW2 model (MAE of 8.7 vs. 8.8 days, respectively), further implying a smaller impact of

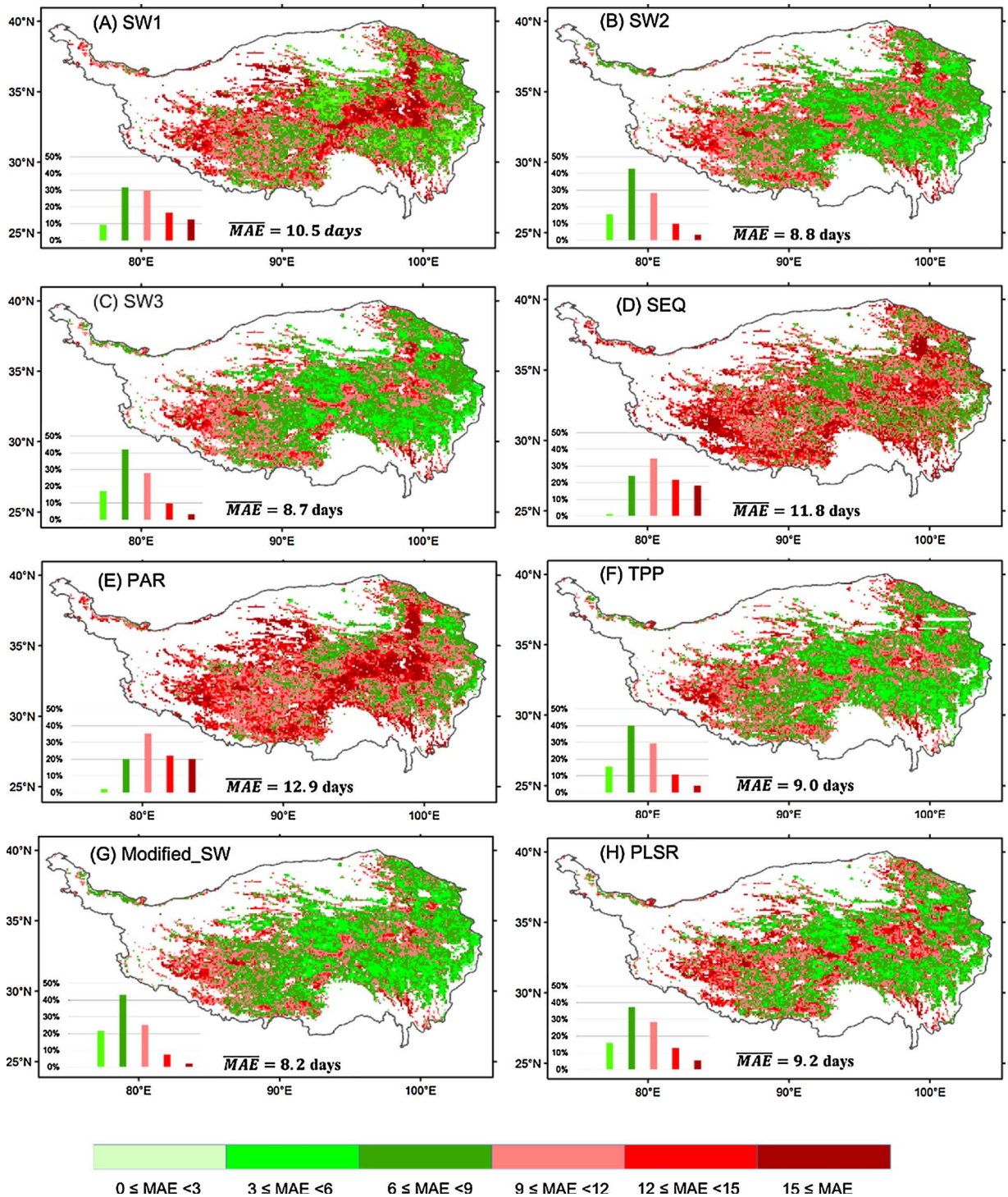

Fig. 3. Mean absolute error (MAE) between simulated and satellite-derived VGDs for SW1 (A), SW2 (B), SW3(C), SEQ (D), PAR(E), TPP (F), the Modified_SW model (G), and the PLSR regression model (H). Inset in each panel is a bar graph of MAEs. Average value of the MAEs appears in each panel.

nighttime mean temperature on heating accumulations for VGD (Fig. 3B and C). The MAEs of the two types of chilling-forcing models were 11.8 days for the SEQ model and 12.9 days for the PAR model (Fig. 3D and E). The SEQ and PAR models involved an additional mechanism, which assumed that lower temperatures in winter caused plants to enter ecodormancy. However, the PLSR analyses showed that winter warming advanced VGD; in addition, the SEQ and PAR models employed daily mean temperature for heating accumulations, both of which might have been responsible for their poor performances. The TPP model did not improve VGD simulations compared with the SW models, although it took into consideration preseason precipitation, as suggested by a number of previous studies (Fig. 3F). The PLSR statistical model achieved moderate accuracy, with a mean MAE of 9.2 days (Fig. 3H). Spatially, the performance of all models, including the Modified_SW model, was worse in the western TP, where the MAE exceeded 12 days.

To quantify the extent to which VGD simulations were improved by embedding a key climate factor in each submodel of the Modified_SW model, we further compared the SW2, SW3, and TPP models with the Modified_SW model for pixels in each of the five cases (Fig. 4). Other

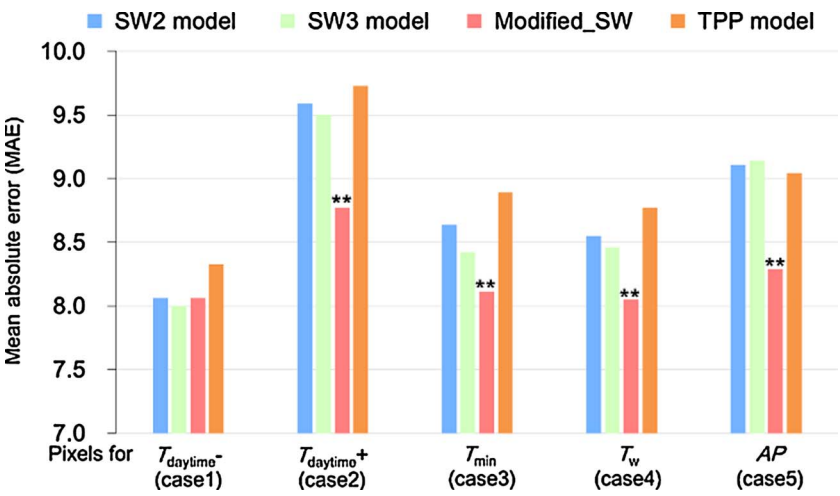

Fig. 4. Comparisons of mean absolute error (MAE) of the SW2, SW3, TPP, and the Modified_SW models for pixels in each case of Fig. 2. ** indicates a difference that is significant at $P < 0.01$ with *t*-test.

models with overall larger errors were not included in this comparison. The Modified_SW model significantly improved VGD simulations in cases 2–5 by considering the influences of daily high and low temperatures, winter temperature, and preseason precipitation, respectively ($P < 0.01$, *t*-test). Compared with SW2, the SW3 model performed significantly better in case 3 ($P < 0.01$), but in the other cases we found no significant differences between SW2 and SW3 ($P = 0.48$, 0.28, 0.37, and 0.73 for cases 1, 2, 4, and 5, respectively; *t*-test for two independent samples). The TPP model achieved a lower MAE compared with both SW models for pixels in case 5, but the difference was not significant (*t*-test, $P = 0.55$), but in the other cases, the performance of the TPP model was obviously worse (Fig. 4). Among the five cases, we found that no matter which model was used, the simulated VGD error was generally larger for case 2. In that case, pixels were identified as having a strong positive correlation between preseason $T_{daytime}$ and VGD. The fact that this positive correlation could not be described by the traditional concept of heat accumulation for vegetation green-up and this may explain the poor performances of the SW2, SW3, and TPP models. The Modified_SW model considered the influence of higher $T_{daytime}$ as a type of stress that increased the heating requirement and reduced VGD simulation errors to an extent.

Fig. 5 shows the spatial patterns of the Pearson's correlations between simulated and satellite-derived VGDs. We found that the Modified_SW model best captured inter-annual variations of VGD across the entire TP, with a positive correlation for 65% of pixels (statistically significant at $P < 0.1$ for 15% of pixels). Negative correlations, however, were also observed, mainly in the western and northwestern TP. These negative correlations highlight the challenge of capturing temporal variations of VGD in localized areas (Fig. 5G). The SW models showed positive correlations in < 50% of pixels, with only 5% being significant ($P < 0.1$) (Fig. 5A–C). The TPP model performed unsatisfactorily across the entire plateau but seemed to capture the inter-annual variations in VGD in the southwestern TP, where preseason precipitation plays an important role in vegetation green-up (Fig. 2 and Fig. 5F). The performances of the SEQ and PAR models were generally the worst among all models (Fig. 5D and E). We further explored the performances of each submodel of the Modified_SW model by counting the percentage of pixels with a positive correlation for each of the five cases (Fig. 6). There was a clear improvement of the Modified_SW model in each case. We thus concluded that the overall improvement of the Modified_SW model was due to involvement of the most important climate factor in each submodel. We also noted that < 30% of pixels showed a positive correlation in case 2, including the Modified_SW model (Fig. 6), the suggestion being that the positive correlation between preseason $T_{daytime}$ and VGD was not sufficiently accounted for by all models.

4. Discussion

Our results were consistent with the hypothesis that VGD on the TP was codetermined by temperature and precipitation. Further, daytime and nighttime temperature in a day showed different effects on VGD, a finding that should be carefully considered in predicting VGDs. The Modified_SW model improved VGD predictions by involving a key climate variable in each submodel. In the regional applications of Modified_SW, the parameter values in the model should be first calibrated at each pixel by using data of previous years and then the parameterized model could be applied to this pixel for the current year. For example, in the Modified_SW model, the histogram of base temperature is skewed towards 0 °C and the starting date for heat accumulation is mainly during day of year 75–120 (i.e. mid-March to end of April) (Fig. S2). So the parameter values in the Modified_SW model should be specified for different pixels. Such treatment is necessary because there could be large errors for regional VGD simulations with an identical parameters (Xin et al., 2015). As far as we know, this is the first effort to simulate spring phenology across the entire TP, although VGD simulations at several separate sites have been conducted in previous studies (Chen et al., 2015).

Asymmetric effects of daytime and nighttime temperature on VGD have been emphasized in recent studies (Fu et al., 2016; Piao et al., 2015; Rossi and Isabel, 2017; Shen et al., 2016). Piao et al. (2015) have recommended daytime temperature for heat accumulation calculations based on evidences from satellite remote sensing observations. Fu et al. (2016) conducted a manipulative warming experiment for three warming treatments: daytime, nighttime or whole-day warming. They found that daytime temperatures be given three times the weight of nighttime temperatures when estimating the effect of temperature on VGD. Our experimental results were consistent with these earlier studies; our VGD simulations were indeed improved by assuming that heat accumulation was a function of mainly daytime temperature (SW2 and SW3 vs. SW1 model) (Fig. 3). However, PLSR analyses clearly showed that increasing T_{min} could greatly advance VGD over as much as 36% of the area of the TP (Fig. 2). What is the explanation for such strong impacts of nighttime low temperatures on VGD? It seems unlikely that this impact is attributable to a direct contribution of nighttime temperature to heat accumulation. We concluded that nighttime low temperatures should be considered a constraint on vegetation green-up, because lower nighttime temperatures may force plants to postpone vegetation green-up to mitigate the risk of frost damage, as suggested by Shen et al. (2016). We thus employed this mechanism in the corresponding submodel of the Modified_SW (i.e., case 3), which assumed that a relatively low T_{min} preceding a day reduced the efficiency of heat accumulation on that day (Table 1). Simulation results showed that this submodel performed significantly better than the SW2 and SW3 models,

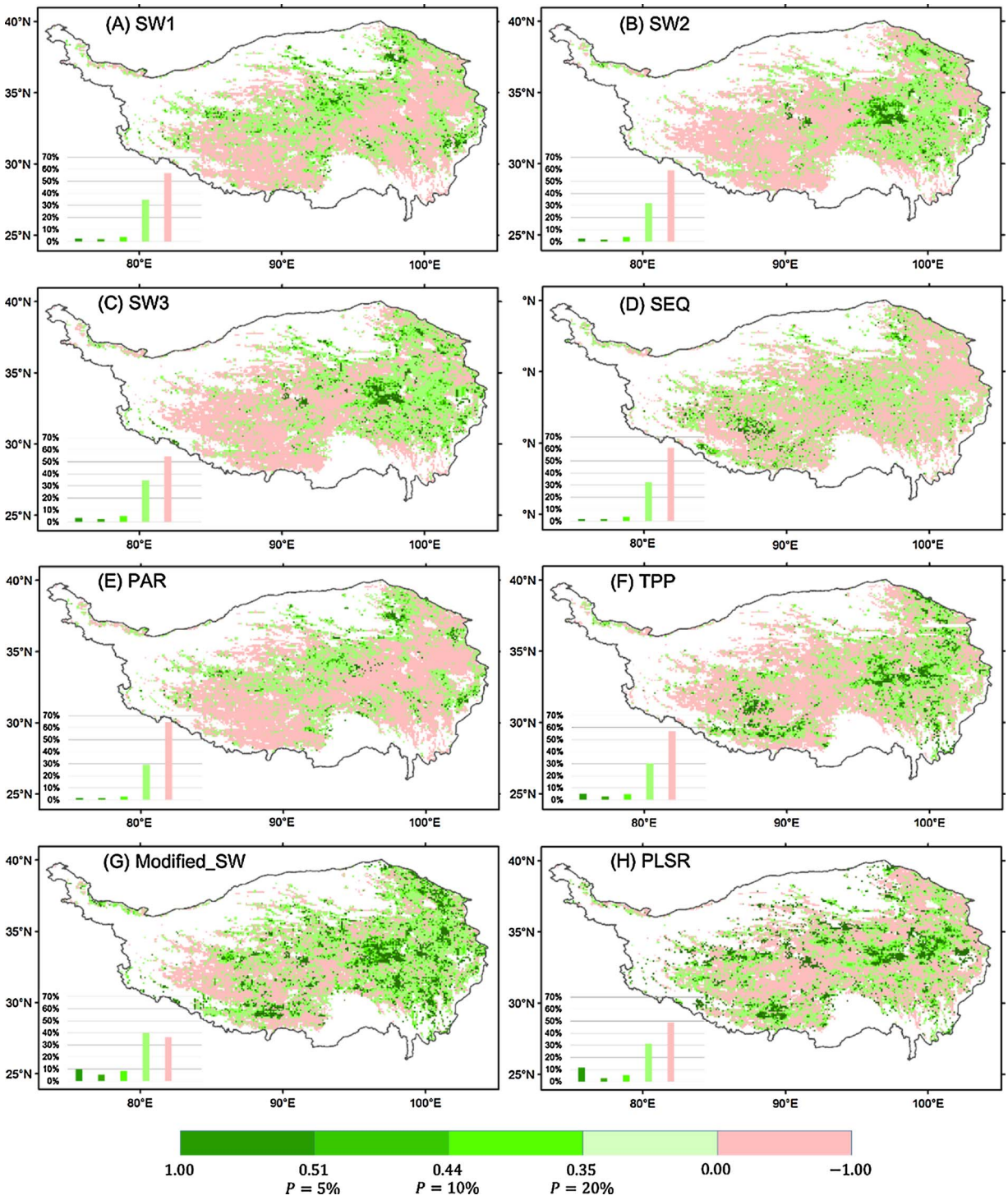

Fig. 5. Spatial patterns of Pearson's correlation coefficients between simulated and satellite-derived VGDs for SW1 (A), SW2 (B), SW3 (C), SEQ (D), PAR (E), TPP (F), the Modified_SW model (G), and the PLSR regression model (H). Inset in each panel is a bar graph of Pearson's correlation coefficients. R = 0.51, 0.44, and 0.35 correspond to the 5%, 10%, and 20%, respectively, significance levels.

which were based mainly on daytime temperature ($P < 0.01$, t-test) (case 3 in Figs. 4 and 6). This result emphasizes that we should consider asymmetric impacts of temperature within a day—that is, the contribution to heat accumulation by daytime mean temperatures and the constraints imposed by low nighttime temperatures on the TP.

Winter mean temperature had the greatest impact on VGD for the lowest percentage of pixels (13%; Fig. 2), and the chilling-forcing models had the largest simulation errors. This result confirms the results of some previous studies that winter temperature is currently not a key climate determinant of VGD on the TP (Chen et al., 2015; Cong et al., 2017; Zhang et al., 2013) and contradicts the hypothesis that winter warming delayed VGD owing to inadequate chilling as suggested by Yu et al. (2010). We explained this as: VGD is not linearly correlated to chilling requirement. Once the chilling requirement is satisfied, extra chilling days exceeding the chilling requirement unit should have no impacts on VGD. On the TP, the winter is long in most areas, and thus the chilling requirement is always fulfilled and has little impact on heat requirement (Cong et al., 2017). However, in a few areas where chilling

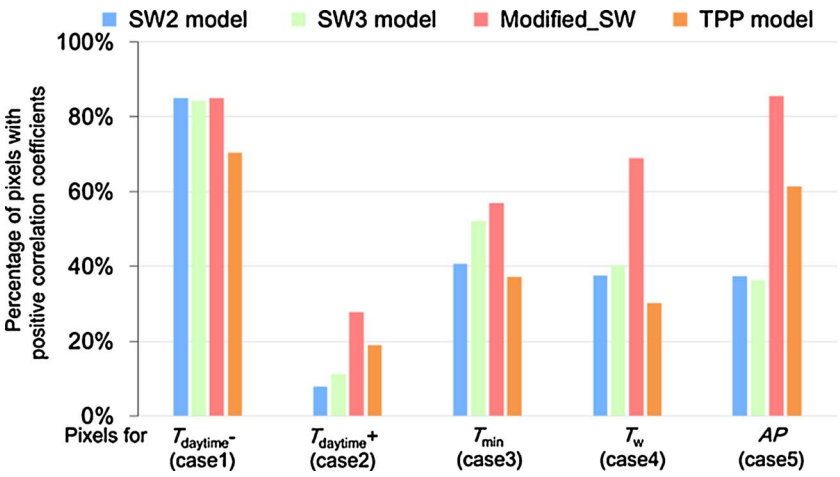

Fig. 6. Comparisons of percentages of pixels with positive Pearson's correlation coefficients for SW2, SW3, TPP, and the Modified_SW model for each case in Fig. 2.

unit is not sufficient, it could have significant impacts on VGD. Because it may be difficult to describe the nonlinear relationships between chilling and winter temperatures, we used T_w directly in the submodel of the Modified_SW to improve VGD simulations.

We found the strongest control of preseason accumulated precipitation on the VGD in the western TP (Figs. 1 and 2). In these localized areas, both the TPP and the Modified_SW models involved *AP* and improved the performances of VGD simulations (Figs. 4 and 6). The fact that the TPP model assumes that *AP*, in addition to temperature, must reach a critical sum of units suggests a direct impact of precipitation on VGD. The scenario in the Modified_SW model, however, is an indirect impact of *AP* based on the assumption that decreasing precipitation increases the heat requirement for VGD. Precipitation probably affects VGD in both direct and indirect ways on the TP (Shen et al., 2015a). The better simulations achieved with the Modified_SW suggest that an indirect impact of precipitation may be a better assumption. One possible explanation is that on the TP water may become available in multiple ways, including from precipitation, spring thaw, snow melting, and permafrost degradation. Without accurate descriptions of water sources, defining a sum of precipitation units to be reached could sometimes lead to errors in VGD model predictions.

We found that the worst simulations involved pixels where the correlations between VGD and $T_{daytime}$ were positive (i.e., case 2 in Figs. 4 and 6). Some previous studies have also observed this positive correlation in grassland ecosystems (e.g., Shen et al., 2016; Yu et al., 2003); the explanation has been that an increase of temperature increases evapotranspiration and hence reduces soil water. If this were the explanation, we would expect that there would be fewer pixels with a positive correlation if we used soil water data in place of precipitation data. We thus employed the root-zone soil moisture data provided by the GLEAM (Global Land Evaporation Amsterdam Model) dataset (http://www.gleam.eu; Miralles et al., 2011). We calculated the partial correlation coefficients between VGD and $T_{daytime}$ for pixels in case 2 by making root-zone soil moisture the controlling variable. We found that the positive correlations between $T_{daytime}$ and VGD persisted (Fig. S4 in Supplemental Materials). Thus direct evidence is still lacking to support the hypothesis that the positive correlations between $T_{daytime}$ and VGD are caused indirectly by the effects of $T_{daytime}$ on evapotranspiration. However, the accuracy of large-scale soil moisture data should be taken care, because these datasets are currently based largely on assimilating microware observations in land-surface models. Friedl et al. (2014) have proposed another potential clue that may help us understand this positive correlation. They discovered that higher preseason temperatures may lead to later VGD because of subtle differences in the process of heat accumulation. Support for this idea would require more robust evidence from well-designed manipulative experiments.

We evaluated the performances of phenological models on the basis of leave-one-out cross validation. We did not adopt the AIC or the small-sample-corrected AICc used by some previous studies (e.g., Migliavacca et al., 2012; Yang et al., 2012). The AIC and AICc consider the balance between goodness-of-fit and model complexity, and they penalize models that have more parameters. However, we found inconsistent evaluations between some models when we used both cross validation and AICc (Fig. S5). For example, the smaller AICc for the PLSR model indicated that this model outperformed the SW2 model (AICc: 57.7 vs. 70.0, $P < 0.01$ for *t*-test), but cross validation showed a better simulation by SW2 (MAE: 8.8 days vs. 9.2 days, $P < 0.01$ for *t*-test). The AIC and AICc penalize complex models on the basis of only the number of model parameters, without carefully considering the structure of the models. The sensitivity of a model to noise depends not only on the number of parameters but also on the structure of the model. This consideration might account for the inconsistency of the evaluations. We recommend using cross validation to evaluate phenological models.

This study investigated VGD across the entire TP on the basis of satellite observations. Our modeling efforts revealed complex controls of multiple environmental variables on VGD in this large alpine ecoregion. Remote sensing is the only way to perform such large-scale investigations. However, it should be kept in mind that a pixel probably contains a number of plant species. Satellite-retrieved VGD represents the average growth of greenness for all plants within a pixel. This definition of greenness is somewhat different from metrics based on observations of individual plants, such as bud break or leaf expansion. That being said, it is more difficult to develop phenological models at the level of pixels, which usually contain dozens of species, than it is for a single species (Tang et al., 2016). There is currently great spatial heterogeneity in the direction and magnitude of VGD change on the TP. VGD advanced during 2001–2015 in the central and eastern TP, whereas there was an obvious delaying trend for VGD in the western TP (Fig. S6). More satellite observations and field phenological experiments are urgently needed to better understand how plants respond to ongoing climate warming on the TP.

5. Conclusions

Climate-driven phenological models are currently embedded as important submodules in dynamic global vegetation models (DGVMs) and global climate models (GCMs), but the great uncertainty of vegetation VGD simulations is one of the main sources of error in DGVMs and GCMs (Jeong et al., 2013; Richardson et al., 2012, 2013). We first assessed the performances of several existing state-of-the-art phenological models in estimating VGD across the TP. We then modified the spring warming model by adding constraints identified by a partial least-squares analysis. The Modified_SW model substantially improved simulations of VGD (lowest MAE: 8.2 days) and captured inter-annual

variations of VGD better than other models. The better performance of the Modified_SW model was attributed to its considerations of asymmetric impacts of temperature within a day on VGD and the constraints imposed by winter temperature and preseason precipitation. Our current research could directly contribute to improving phenological submodels and the predictions of vegetation activity across the TP, where extraordinary warming is projected to continue. Nevertheless, although the Modified_SW model is the best predictor of VGD on the TP, the correlation coefficient for simulating inter-annual variations of VGD is low, especially in the western TP. This poor correlation highlights the challenge of developing phenological models that better represent phenology in future ecosystem models.

Acknowledgments

This work was funded by grants from the National Natural Science Foundation of China (No. 41601381, No. 41571103 and No. 91647104), Fundamental Research Funds for the Central Universities (No. ZYGX2015KYQD048) and the Key Research Program of Frontier Sciences of Chinese Academy of Sciences (No. QYZDB-SSW-DQC025).

Appendix A. Supplementary data

Supplementary data associated with this article can be found, in the online version, at https://doi.org/10.1016/j.agrformet.2017.11.032.

References

Botta, A., Viovy, N., Ciais, P., Friedlingstein, P., Monfray, P., 2000. A global prognostic scheme of leaf onset using satellite data. Global Change Biol. 6 (7), 709–725.
Cao, R.Y., Chen, J., Shen, M.G., Tang, Y.H., 2015. An improved logistic method for detecting spring vegetation phenology in grasslands from MODIS EVI time-series data. Agric. For. Meteorol. 200, 9–20.
Chen, Y.Y., Yang, K., He, J., et al., 2011. Improving land surface temperature modeling for dry land of China. J. Geophys. Res. 116, D20104. http://dx.doi.org/10.1029/2011JD015921.
Chen, X.Q., Li, J., Xu, L., Liu, L., Ding, D., 2014. Modeling greenup date of dominant grass species in the Inner Mongolian Grassland using air temperature and precipitation data. Int. J. Biometeorol. 58, 463–471.
Chen, X.Q., An, S., Inouye, D.W., Schwartz, M.D., 2015. Temperature and snowfall trigger alpine vegetation green-up on the world's roof. Global Change Biol. 21, 3635–3646.
Chuine, I., Cour, P., Rousseau, D.D., 1998. Fitting models predicting dates of flowering of temperate-zone trees using simulated annealing. Plant Cell Environ. 21, 455–466.
Cleland, E., Chuine, I., Menzel, A., Mooney, H., Schwartz, M., 2007. Shifting plant phenology in response to global change. Trends Ecol. Evol. 22, 357–365.
Cong, N., Shen, M.G., Piao, S.L., et al., 2017. Little change in heat requirement for vegetation green-up on the Tibetan Plateau over the warming period of 1998–2012. Agric. For. Meteorol. 232, 650–658.
Deng, H., Pepin, N.C., Chen, Y., 2017. Changes of snowfall under warming in the Tibetan Plateau. J. Geophys. Res.: Atmospheres 122. http://dx.doi.org/10.1002/2017JD026524.
Forkel, M., Migliavacca, M., Thonicke, K., et al., 2015. Codominant water control on global interannual variability and trends in land surface phenology and greenness. Global Change Biol. 21, 3414–3435.
Friedl, M.A., Gray, J.M., Melaas, E.K., et al., 2014. A tale of two springs: using recent climate anomalies to characterize the sensitivity of temperate forest phenology to climate change. Environ. Res. Lett. 9, 054006.
Fu, Y.H., Zhao, H., Piao, S., et al., 2015. Declining global warming effects on the phenology of spring leaf unfolding. Nature 526, 104–107.
Fu, Y.H., Liu, Y.J., De Boeck, H.G., et al., 2016. Three times greater weight of daytime than of night-time temperature on leaf unfolding phenology in temperate trees. New Phytologist 212, 590–597.
Ganguly, S., Friedl, M.A., Tan, B., et al., 2010. Land surface phenology from MODIS: characterization of the Collection 5 global land cover dynamics product. Remote Sens. Environ. 114, 1805–1816.
Hanes, J.M., 2014. Spring leaf phenology and the diurnal temperature range in a temperate maple forest. Int. J. Biometeorol. 58, 103–108.
Huffman, G.J., Adler, R.F., Bolvin, D.T., et al., 2007. The TRMM multisatellite precipitation analysis (TMPA): quasi-global, multiyear: combined-sensor precipitation estimates at fine scales. J. Hydrometeorol. 8, 38–55.
Jeong, S.J., Medvigy, D., Shevliakova, E., Malyshev, S., 2012. Uncertainties in terrestrial carbon budgets related to spring phenology. J. Geophys. Res. 117, G01030.
Jeong, S.J., Medvigy, D., Shevliakova, E., Malyshev, S., 2013. Predicting changes in temperate forest budburst using continental-scale observations and models. Geophys. Res. Lett. 40, 359–364. http://dx.doi.org/10.1029/2012GL054431.
Körner, C., Basler, D., 2010. Phenology under global warming. Science 327, 1461–1462.
Keenan, T.F., Gray, J., Friedl, M.A., et al., 2014. Net carbon uptake has increased through warming-induced changes in temperate forest phenology. Nat. Clim. Change 4, 598–604.
Kramer, K., 1994. Selecting a model to predict the onset of growth of Fagus sylvatica. J. Appl. Ecol. 31, 172–181. http://dx.doi.org/10.2307/2404609.
Linkosalo, T., Lappalainen, H.K., Hari, P., 2008. A comparison of phenological models of leaf bud burst and flowering of boreal trees using independent observations. Tree Physiol. 28, 1873–1882.
Menzel, A., Fabian, P., 1999. Growing season extended in Europe. Nature 397, 659.
Migliavacca, M., Sonnentag, O., Keenan, T.F., et al., 2012. On the uncertainty of phenological responses to climate change, and implications for a terrestrial biosphere model. Biogeosciences 9 (6), 2063–2083 (10.5194/bg-9-2063-2012).
Miralles, D.G., Holmes, T.R.H., De Jeu, R.A.M., et al., 2011. Global land-surface evaporation estimated from satellite-based observations. Hydrol Earth Syst. Sci. 15, 453–469 (10.5194/hess-15-453-2011).
Murray, M.B., Cannell, M.G.R., Smith, R.I., 1989. Date of budburst of 15 tree species in Britain following climatic warming. J. Appl. Ecol. 26, 693–700.
Parmesan, C., 2006. Ecological and evolutionary responses to recent climate change. Annu. Rev. Ecol. Evol. Syst. 37, 637–669.
Peñuelas, J., Rutishauser, T., Fiella, I., 2009. Phenology feedbacks on climate change. Science 324, 887–888.
Piao, S.L., Cui, M., Chen, A., et al., 2011. Altitude and temperature dependence of change in the spring vegetation green-up date from 1982 to 2006 in the Qinghai–Xizang Plateau. Agric. For. Meteorol. 151, 1599–1608.
Piao, S.L., Tan, J.G., Chen, A., et al., 2015. Leaf onset in the northern hemisphere triggered by daytime temperature. Nat. Commun. 6, 6911.
Richardson, A.D., Anderson, R.S., Arain, M.A., et al., 2012. Terrestrial biosphere models need better representation of vegetation phenology: results from the North American Carbon Program Site Synthesis. Global Change Biol. 18, 566–584.
Richardson, A.D., Keenan, T.F., Migliavacca, M., et al., 2013. Climate change, phenology, and phenological control of vegetation feedbacks to the climate system. Agric. For. Meteorol. 169, 156–173.
Rossi, S., Isabel, N., 2017. Bud break responds more strongly to daytime than night-time temperature under asymmetric experimental warming. Global Change Biol. 23 (1), 446–454.
Schaaf, C.G., Gao, F., Strahler, A.H., et al., 2002. First operational BRDF: albedo nadir reflectance products from MODIS. Remote Sens. Environ. 83, 135–148.
Sheffield, J., Goteti, G., Wood, E.F., 2006. Development of a 50-year high-resolution global dataset of meteorological forcings for land surface modeling. J. Clim. 19, 3088–3111.
Shen, M.G., Tang, Y.H., Chen, J., et al., 2011. Influence of temperature and precipitation before the growing season on spring phenology in grasslands of the central and eastern Qinghai-Tibetan Plateau. Agric. For. Meteorol. 151, 1711–1722.
Shen, M.G., Zhang, G.X., Cong, N., et al., 2014. Increasing altitudinal gradient of spring vegetation phenology during the last decade on the Qinghai-Tibetan Plateau. Agric. For. Meteorol. 180–190, 71–80.
Shen, M.G., Piao, S.L., Cong, N., Zhang, G.X., Jassens, I.A., 2015a. Precipitation impacts on vegetation spring phenology on the Tibetan Plateau. Global Change Biol. 21, 3647–3656.
Shen, M.G., Piao, S.L., Dorji, T., et al., 2015b. Plant phenological responses to climate change on the Tibetan Plateau: research status and challenges. Natl. Sci. Rev. 22, 454–467.
Shen, M.G., Piao, S.L., Chen, X.Q., et al., 2016. Strong impacts of daily minimum temperature on the green-up date and summer greenness of the Tibetan Plateau. Global Change Biol. 22, 3057–3066.
Tang, J.W., Körner, C., Muraoka, H., et al., 2016. Emerging opportunities and challenges in phenology: a review. Ecosphere 7, e01436.
Vitasse, Y., François, C., Delpierre, N., et al., 2011. Assessing the effects of climate change on the phenology of European temperate trees. Agric. For. Meteorol. 151, 969–980. http://dx.doi.org/10.1016/j.agrformet.2011.03.003.
Walther, G.R., Post, E., Convey, P., et al., 2002. Ecological responses to recent climate change. Nature 416, 389–395.
Wang, H., Liu, D., Lin, H., Montenegro, A., Zhu, X., 2015. NDVI and vegetation phenology dynamics under the influence of sunshine duration on the Tibetan plateau. Int. J. Climatol. 35, 687–698.
Wold, S., 1995. PLS for multivariate linear modeling. chemometric methods in molecular design. In: In: van der Waterbeemd, H. (Ed.), Methods and Principles in Medicinal Chemistry 2. Verlag-Chemie, Weinheim, Germany, pp. 195–218.
Wu, C., Hou, X., Peng, D., Gonsamo, A., Xu, S., 2016. Land surface phenology of China's temperate ecosystems over 1999–2013 Spatial–temporal patterns, interaction effects, covariation with climate and implications for productivity. Agric. For. Meteorol. 216, 177–187.
Xin, Q.C., Broich, M., Zhu, P., Gong, P., 2015. Modeling grassland spring onset across the Western United States using climate variables and MODIS-derived phenology metrics. Remote Sens. Environ. 161, 63–77.
Yang, K., He, J., Tang, W.J., Qin, J., Cheng, C.C.K., 2010. On downward shortwave and longwave radiations over high altitude regions: observation and modeling in the Tibetan Plateau. Agric. For. Meteorol. 150, 38–46.
Yang, X., Mustard, J.F., Tang, J.W., Xu, H., 2012. Regional-scale phenology modeling based on meteorological records and remote sensing observations. J. Geophys. Res. 117 (G3), 1–18.
Yatagai, A., Arakawa, O., Kamiguchi, K., et al., 2009. A 44-year daily gridded precipitation dataset for Asia based on a dense network of rain gauges. Sola 5, 137–140.
Yu, F.F., Price, K.P., Ellis, J., et al., 2003. Response of seasonal vegetation development to climatic variations in eastern central Asia. Remote Sens. Environ. 87, 42–54.
Yu, H.Y., Luedeling, E., Xu, J.C., 2010. Winter and spring warming result in delayed spring phenology on the Tibetan Plateau. Proc. Natl. Acad. Sci. U. S. A. 107,

22151–22156.
Zhang, X.Y., Friedl, M.A., Schaaf, C.B., et al., 2003. Monitoring vegetation phenology using MODIS. Remote Sens. Environ. 84, 471–475.
Zhang, X.Y., Friedl, M.A., Schaaf, C.B., 2006. Global vegetation phenology from Moderate Resolution Imaging Spectroradiometer (MODIS): evaluation of global patterns and comparison with in situ measurements. J. Geophys. Res. 111 (G4), G04017.
Zhang, J., Wu, L., Huang, G., Zhu, W., Zhang, Y., 2011. The role of May vegetation greenness on the southeastern Tibetan Plateau for East Asian summer monsoon prediction. J. Geophys. Res. 116. http://dx.doi.org/10.1029/2010JD015095.
Zhang, G.L., Zhang, Y.J., Dong, J.W., Xiao, X.M., 2013. Green-up dates in the Tibetan Plateau have continuously advanced from 1982 to 2011. Proc. Natl. Acad. Sci. U. S. A. 110, 4309–4314.
Zheng, Z.T., Zhu, W.Q., Chen, G.S., et al., 2016. Continuous but diverse advancement of spring-summer phenology in response to climate warming across the Qinghai-Tibetan Plateau. Agric. For. Meteorol. 223, 194–202.
Zhu, W.Q., Tian, H.Q., Xu, X.F., et al., 2012. Extension of the growing season due to delayed autumn over mid and high latitudes in North America during 1982–2006. Global Ecol. Biogeogr. 21, 260–271.